



Original article

Impact of suction and thermal radiation on unsteady ternary hybrid nanofluid flow over a biaxial shrinking sheet

Nur Syahirah Wahid^{a,*}, Norihan Md Arifin^{a,b}, Rusya Iryanti Yahaya^b,
Najiyah Safwa Khashi'ie^c, Ioan Pop^{d,e}

^a Department of Mathematics and Statistics, Faculty of Science, Universiti Putra Malaysia, 43400 UPM, Serdang, Selangor, Malaysia

^b Institute for Mathematical Research, Universiti Putra Malaysia, 43400 UPM, Serdang, Selangor, Malaysia

^c Fakulteti Teknologji dhe Kejuruteraan Mekanikal, Universiti Teknikal Malaysia Melaka, Hang Tuah Jaya, Durian Tunggal, Melaka 76100, Malaysia

^d Department of Mathematics, Babeş-Bolyai University, Cluj-Napoca R-400084, Romania

^e Academy of Romanian Scientists, 3 Ilfov Street, Bucharest 050044, Romania.

ARTICLE INFO

Keywords:

Ternary hybrid nanofluid

Shrinking

Thermal radiation

Unsteady flow

ABSTRACT

The use of hybrid nanofluids in practical applications is pivotal for enhanced heat transfer efficiency especially for electronics cooling, and manufacturing processes. This study delves into numerically investigating the unsteady water-based (alumina+copper+titanium dioxide) ternary hybrid nanofluid flow over a permeable biaxial shrinking sheet, considering the influence of thermal radiation. The model, initially formulated as partial differential equations (PDEs), is adeptly transformed into ordinary differential equations (ODEs) via established similarity transformations. Subsequently, a numerical solution employing the finite difference scheme in bvp4c MATLAB unravels the behaviors of crucial physical quantities—across various parameter configurations. Remarkably, this study reveals the presence of two potential solutions, among which only one exhibits physical stability. Notably, the findings underscore the efficacy of enlarging the boundary suction parameter and diminishing thermal radiation for augmenting heat transfer within the specified conditions of ternary hybrid nanofluid. A noteworthy finding of this study reveals that an increase in the boundary suction parameter by 4% leads to a remarkable 9% delay in the boundary layer separation of the ternary hybrid nanofluid, thus maintaining the laminar phase flow. This study offers crucial guidance and insights for researchers and practitioners delving into the mathematical or experimental aspects of ternary hybrid nanofluid dynamics.

1. Introduction

A hybrid nanofluid constitutes a composite amalgamation comprising two discrete nanoparticles dispersed within a base fluid. The combination of dissimilar nanoparticles integrates various material properties to reduce the drawback of a single suspension nanofluid. Hence, it forms an exceptionally proficient heat transfer agent with notably enhanced thermophysical attributes compared to both traditional fluids and nanofluids. Recently, a novel ternary hybrid nanofluid has been developed, incorporating the dissemination of three diverse nanoparticles within a base fluid. This innovative fluid is anticipated to demonstrate heightened thermophysical properties, surpassing those observed in both hybrid nanofluids and single nanofluids. Various experimental and theoretical studies have been performed to understand the flow and thermal properties of this fluid, as well as its potential as a

substitute for conventional heat transfer fluids used in diverse applications such as technological processes, pharmaceutical operations, fuel cells, microelectronics, drug delivery systems, automobile coolants, nuclear reactor cooling, and thermal storage [1,2]. An in-depth analysis of the preparation, stability, thermophysical properties, and environmental effects of ternary hybrid nanofluid can be seen in the review paper by Adun et al. [3].

In the context of ternary hybrid nanofluid, based on previous studies, Elnaqeeb et al. [4] analyzed the suction effect on ternary hybrid nanofluid flow with varied nanoparticle geometries and densities in a rectangular closed area. A higher heat transfer rate was obtained with heavy-density nanoparticles. Some experimental studies were also conducted to understand the rheological properties of ternary hybrid nanofluid in various applications, see [5–7]. Then, Bilal et al. [8] performed a numerical investigation on ternary hybrid nanofluid flow with various shapes such as planes, sheets, cones, and wedges, with the

* Corresponding author.

E-mail address: syahirahwahid@upm.edu.my (N.S. Wahid).

<https://doi.org/10.1016/j.aej.2024.03.079>

Received 3 January 2024; Received in revised form 19 March 2024; Accepted 22 March 2024

Available online 9 April 2024

1110-0168/© 2024 The Author(s). Published by Elsevier BV on behalf of Faculty of Engineering, Alexandria University This is an open access article under the CC BY-NC-ND license (<http://creativecommons.org/licenses/by-nc-nd/4.0/>).

Nomenclatures		Greek Symbols	
C_{fx}, C_{fy}	Skin friction coefficients	β	Unsteadiness parameter
f, g	Dimensionless momentum function	γ	Eigenvalue
k^*	Mean absorption constant	η	Dimensionless variable
k_{thnf}	Thermal conductivity of ternary hybrid nanofluid	θ	Dimensionless temperature function
Nu_x	Local Nusselt number	$\lambda(< 0)$	Shrinking parameter
Pr	Prandtl number	μ_{thnf}	Dynamic viscosity of ternary hybrid nanofluid
Rd	Radiation parameter	ρ_{thnf}	Density of ternary hybrid nanofluid
Re_x, Re_y	Local Reynolds numbers	$(\rho C_p)_{thnf}$	Heat capacitance of ternary hybrid nanofluid
$S(> 0)$	Suction parameter	σ^*	Stefan–Boltzmann constant
t	Time	τ	Dimensionless time variable
T	Temperature	ϕ	Nanoparticle volume fraction
T_w	Sheet temperature	Subscripts	
T_∞	Far-field temperature	$thnf$	Ternary hybrid nanofluid
U	Far-field velocity	hnf	Hybrid nanofluid
u, v, w	Velocities along x, y, z -axes	nf	Nanofluid
u_w, v_w	Sheet velocities	f	Base fluid
w_w	Mass flux velocity	1	Alumina nanoparticle
x, y, z	Cartesian coordinates	2	Copper nanoparticle
		3	Titanium dioxide nanoparticle

inclusion of a magnetic field. During their research, it was observed that the propagation rates of velocity and energy over the cone exceeded those seen over the wedge and plate. Mahmood et al. [9] studied the stagnation-point ternary hybrid nanofluid flow over a convective stretch/shrink cylinder, revealing a notably heightened heat transfer rate compared to both the hybrid nanofluid and nanofluid. This finding aligned with similar results provided by Manjunatha et al. [10] and Mahmood et al. [11] in their respective examinations of ternary hybrid nanofluid flow over stretch/shrink surface. Nandi and Vajravelu [12] found that an increased Weissenberg number in the Carreau ternary hybrid nanofluid flow over a stretch sheet reduced the velocity profile. Zeeshan et al. [13] studied the flow of Casson ternary hybrid nanofluid over a shrinkable sheet subjected to radiation. Their findings show that augmenting the concentration and radiation parameters led to an elevation of the temperature profile. Recently, Riaz et al. [14], Nagaraja et al. [15], Mumtaz et al. [16], and Jan et al. [17] analyzed the flow of ternary hybrid nanofluid across a stretch sheet with various flow conditions.

Thermal radiation is one of the three modes of heat transmission that operates independently of the intervening medium. Unlike conduction and convection, which rely on the transfer of energy through a physical medium, thermal radiation occurs through electromagnetic waves [18]. Thermal radiation is the emission of electromagnetic radiation from a material, driven by its temperature, and the characteristics of the radiation are determined by the heat of the material [19]. The distribution of temperatures in various applications, especially those involving dissociating fluids and chemical reactions like space vehicle re-entry, astrophysical flows, electrical power generation, optoelectronics technology, spectroscopy, and solar power technology, can be altered by thermal radiation [20,21]. This parameter has been considered widely by researchers in modeling the heat transfer in boundary layer flow. For example, Mishra et al. [22] investigated the rotational nanofluid flow over an elongating sheet with thermal radiation. Pal and Mandal [23] studied the hybrid nanofluid flow over a shrinkable surface with Ohmic heating and radiation effect. The radiation effect has also been considered by Alqahtani et al. [24] in their study on electrically conducting a spinning flow of hybrid nanofluid across two parallel surfaces, and they concluded that the increment of radiation could enhance the temperature distribution of the fluid. The same conclusion also has been drawn by Swain et al. [25] on the fluid flow problem regarding the radiative flow of Maxwell fluid over a permeable stretching surface with a heat

source/sink. Later, Alharbi et al. [26] studied the stagnation point flow of hybrid nanofluid flow passing over a rotating sphere subjected to thermophoretic diffusion with the inclusion of thermal radiation. The heat transfer rate of their model is seen to improve with the increment of thermal radiation. Recently, Hamad et al. [27] also found out that the temperature profile is elevated with the inclusion of radiation effect in their study on third-grade fluid flow across an inclined stretching sheet with Lorentz force. For overall, it is noticed that the inclusion of thermal radiation is generally aid in increasing the temperature distribution of the fluid flow model even when the models exhibit some variation. Incorporating thermal radiation into fluid flow models is essential to achieve precise and authentic temperature predictions, especially in situations involving high temperatures or combustion. This inclusion facilitates a more comprehensive portrayal of the underlying physical phenomena in the heat transfer process.

A biaxially stretchable surface within boundary layer flow involves a surface that extends in two perpendicular directions simultaneously. In fluid mechanics, a critical aspect involves examining the reaction of fluids to stretching or deformation on surfaces. This concept helps analyze alterations in boundary layer thickness, velocity profiles, and shear stresses due to such stretching, holding significant importance in disciplines such as material science and aerodynamics. The utilization of biaxially stretching and shrinking sheets is widespread in industrial applications, encompassing packaging films, heat shrink labels, synthetic fibers, and stretchable materials in the automotive and medical sectors. Historically, Wang [28] carried out an investigation focusing on the three-dimensional (3D) flow of fluid over a biaxially stretchable surface, wherein exact similarity solutions derived from the Navier-Stokes equations were presented. Later, the flow of nanofluid and hybrid nanofluid over biaxial stretch/shrink surface was examined by other researchers. Mahanthesh et al. [29] reported the numerical solution for nanofluid flow over a biaxial stretch surface with a magnetic effect and variable surface heat flux. Then, the radiative Maxwell nanofluid flow over a biaxial porous stretch surface was studied by Ramesh et al. [30] with a heat source/sink. Next, Ahmad et al. [31] considered the magnetic effect on nanofluid flow over a biaxial stretch surface within a porous media. Additional investigations concerning nanofluid flow over a biaxially stretchable surface have also been undertaken as in [32–36]. Meanwhile, Groşan and Pop [37] analyzed the nanofluid flow past a biaxial stretch/shrink sheet and dual solutions were discovered when the sheet was shrunk in the horizontal direction.

Khashi'ie et al. [38] discussed the nanofluid flow over a biaxial shrinkable sheet. It was concluded that suction is needed to generate the solution for the opposing flow case. Research on hybrid nanofluid flow over a biaxially stretchable/shrinkable sheet has been explored in studies conducted by various researchers, including Waini et al. [39], Zainal et al. [40], and Yasir et al. [41]. Yahaya et al. [42] recently presented the heat transfer optimization for radiative hybrid nanofluid flow past permeable biaxial stretch/shrink surface and it was found that the suction parameter impacts the heat transfer rate positively. Besides that, the flow of ternary hybrid nanofluid over a biaxial stretch sheet has been studied by Manjunatha et al. [43]. The study also accounted for convective boundary conditions and velocity slip. Recently, the Casson ternary hybrid nanofluid flow over a biaxial stretch sheet with magnetic field, radiation, viscous dissipation, and heat source/sink was examined by Choudhary et al. [44].

From these earlier investigations, there is a severe scarcity of research dedicated to examining the behavior of ternary hybrid nanofluids over biaxially shrinking sheets, particularly when focusing on the unsteady flow dynamics, especially in the case of alumina-copper-titanium dioxide ternary hybrid nanofluids. Therefore, this current study intends to model and solve the unsteady flow of ternary hybrid nanofluid over a permeable biaxially shrinkable sheet with thermal radiation. This study is based on prior research by Wang [45], Khashi'ie et al. [38], and Yahaya et al. [42] which is improved to the unsteady flow case with the consideration of ternary hybrid nanofluid. It should be noted that these mentioned previous studies do not consider the unsteady flow of ternary hybrid nanofluid but instead just the steady flow of classical fluid, single nanofluid, and hybrid nanofluid. For the model formulation, the introduction of the governing PDEs and boundary conditions for the flow problem will be followed by the application of appropriate similarity transformations which convert the equations into nonlinear ODEs. Ultimately, the ODEs are solved numerically in MATLAB to compute the numerical solution of interest. All tabulated and illustrated solutions are analyzed and discussed.

1.1. Novelty of the study

The novelties of the present study are as follows:

- This study delves into optimizing heat transfer performance of ternary hybrid nanofluid through manipulation of suction and thermal radiation parameters.
- Provides guidance on achieving maximum heat transfer efficiency while controlling boundary layer separation in ternary hybrid nanofluids.
- Highlight the impact of thermal radiation and suction on unsteady ternary hybrid nanofluid flow over a permeable biaxial shrinking sheet specifically in terms of skin friction, heat transfer rate, velocity, and temperature.

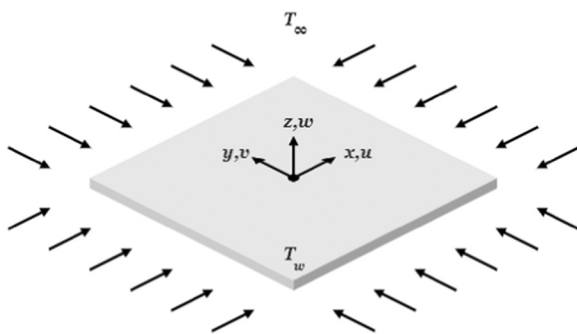


Fig. 1. Coordinated physical model.

1.2. Research questions

At the end of this study, some of the research questions that we aim to answer are as follows:

- How can boundary suction parameters and thermal radiation be effectively utilized to optimize heat transfer in ternary hybrid nanofluid?
- What is the influence of alterations in suction parameters on local skin friction, boundary layer separation, velocity, and temperature of the ternary hybrid nanofluid?
- How does thermal radiation impact the temperature distribution within the ternary hybrid nanofluid system?
- Does the thermal radiation affect the boundary layer separation process of the ternary hybrid nanofluid?

2. Mathematical modeling

To model and solve the unsteady 3D boundary layer flow of a ternary hybrid nanofluid across a permeable biaxial shrinking sheet influenced by thermal radiation is the goal of the present study. The sheet lies on the x, y -plane, with (x, y, z) serving as Cartesian coordinates, where the z -axis stands normal to the x, y -plane, while flow resides within $z \geq 0$ (see Fig. 1). The sheet shrunk both in the x, y directions while maintaining a stationary point of origin. Further assumptions are detailed as follows:

- The velocities of the sheet are $u_w(x, t) = ax/(1 - ct)$ and $v_w(y, t) = ay/(1 - ct)$, respective to x - and y -directions, with constant $a(> 0)$ and time t .
- The variable mass flux velocity is $w_w(t)$ where $w_w(t) < 0$ is for suction.
- The sheet maintains a constant temperature of T_w , while the temperature in the far field remains T_∞ .
- The thermal radiation parameter is given by $16\sigma^* T_\infty^3/3k^*$ where σ^* and k^* are the Stefan–Boltzmann constant and mean absorption constant, respectively.
- To enhance thermal properties, three distinct nanoparticles—alumina, copper, and titanium dioxide—are taken into account, each diluted within the base fluid water.

From the aforementioned assumptions, we can express the boundary layer equations, as below (see Wang [45]; Devi and Devi [46]; Yahaya et al. [42];):

$$\frac{\partial u}{\partial x} + \frac{\partial v}{\partial y} + \frac{\partial w}{\partial z} = 0, \quad (1)$$

$$\frac{\partial u}{\partial t} + u \frac{\partial u}{\partial x} + v \frac{\partial u}{\partial y} + w \frac{\partial u}{\partial z} = \frac{\mu_{thnf}}{\rho_{thnf}} \frac{\partial^2 u}{\partial z^2}, \quad (2)$$

$$\frac{\partial v}{\partial t} + u \frac{\partial v}{\partial x} + v \frac{\partial v}{\partial y} + w \frac{\partial v}{\partial z} = \frac{\mu_{thnf}}{\rho_{thnf}} \frac{\partial^2 v}{\partial z^2}, \quad (3)$$

$$\frac{\partial w}{\partial t} + u \frac{\partial w}{\partial x} + v \frac{\partial w}{\partial y} + w \frac{\partial w}{\partial z} = \frac{\mu_{thnf}}{\rho_{thnf}} \frac{\partial^2 w}{\partial z^2}, \quad (4)$$

$$\frac{\partial T}{\partial t} + u \frac{\partial T}{\partial x} + v \frac{\partial T}{\partial y} + w \frac{\partial T}{\partial z} = \frac{1}{(\rho C_p)_{thnf}} \left(k_{thnf} + \frac{16\sigma^* T_\infty^3}{3k^*} \right) \frac{\partial^2 T}{\partial z^2}, \quad (5)$$

subject to the boundary conditions [38,47]:

$$\left. \begin{aligned} t < 0 : u = v = w = 0, T = T_{\infty} \text{ for any } x, y, z, \\ t \geq 0 : u = \frac{u_w(x)}{1-ct} \lambda = \frac{ax}{1-ct} \lambda, v = \frac{v_w(y)}{1-ct} \lambda = \frac{ay}{1-ct} \lambda, w = w_w, T = T_w \text{ at } z = 0, \\ u = u_e \rightarrow U, v = v_e \rightarrow 0, T \rightarrow T_{\infty} \text{ as } z \rightarrow \infty. \end{aligned} \right\} \quad (6)$$

Within these equations, (u, v, w) represent the velocities aligned with (x, y, z) -axes, while T signifying the temperature of the hybrid nanofluids. Additionally, U denotes the far field velocity of the ternary hybrid nanofluid, and $\lambda (< 0)$ stands for the shrinking parameter. The thermophysical properties of the ternary hybrid nanofluid are delineated in Table 1, encompassing parameters such as μ_{thnf} , representing dynamic viscosity; ρ_{thnf} , denoting density; k_{thnf} , indicating thermal conductivity; and $(\rho C_p)_{thnf}$, signifying the heat capacitance of the hybrid nanofluid.

Here, ϕ is the nanoparticle volume fraction while the suffix *thnf*, *hnf*, *nf*, and *f* are for the ternary hybrid nanofluid, hybrid nanofluid, nanofluid, and the base fluid, while the suffixes 1, 2, and 3 refer to alumina, copper, and titanium dioxide. The thermophysical properties of each nanoparticle and the base fluid, which are outlined in Table 2, adhere to the conservation principles of mass and energy, forming correlations rooted in physical assumptions.

Similar to Wang [45], it is appropriate to present the subsequent similarity variables:

$$\left. \begin{aligned} u = \frac{1}{1-ct} [axf'(\eta) + Uh(\eta)], v = \frac{ay}{1-ct} g'(\eta), w = -\sqrt{\frac{av_f}{1-ct}} [f(\eta) + g(\eta)], \\ \theta(\eta) = \frac{T - T_{\infty}}{T_w - T_{\infty}}, \eta = z \sqrt{\frac{a}{v_f(1-ct)}}, \end{aligned} \right\} \quad (7)$$

and also,

$$w_w(t) = -\sqrt{\frac{av_f}{1-ct}} S. \quad (8)$$

The prime notation signifies differentiation concerning η . Meanwhile, S denotes the constant mass flux velocity, such that $S > 0$ is for suction.

Upon satisfaction of the continuity Eq. (1) by the similarity variables (7), the act of substituting (7) into Eqs. (2)–(6) results in the following ODEs:

$$\left(\frac{\mu_{thnf}}{\rho_{thnf}} \frac{\mu_f}{\rho_f} \right) f''' + (f + g)f'' - f'^2 - \beta \left(f' + \frac{1}{2} \eta f'' \right) = 0, \quad (9)$$

$$\left(\frac{\mu_{thnf}}{\rho_{thnf}} \frac{\mu_f}{\rho_f} \right) g''' + (f + g)g'' - g'^2 - \beta \left(g' + \frac{1}{2} \eta g'' \right) = 0, \quad (10)$$

$$\left(\frac{\mu_{thnf}}{\rho_{thnf}} \frac{\mu_f}{\rho_f} \right) h'' + (f + g)h' - hf' - \beta \left(h + \frac{1}{2} \eta h' \right) = 0, \quad (11)$$

Table 1
Thermophysical properties of ternary hybrid nanofluid [10].

Properties	Formulations
Dynamic viscosity	$\mu_{thnf} = \frac{\mu_f}{(1-\phi_1)^{2.5}(1-\phi_2)^{2.5}(1-\phi_3)^{2.5}}$
Density	$\rho_{thnf} = (1-\phi_1)\{(1-\phi_2)[(1-\phi_3)\rho_f + \phi_3\rho_3] + \phi_2\rho_2\} + \phi_1\rho_1$
Heat capacitance	$(\rho C_p)_{thnf} = (1-\phi_1)\{(1-\phi_2)[(1-\phi_3)\rho_f + \phi_3(\rho C_p)_3] + \phi_2(\rho C_p)_2\} + \phi_1(\rho C_p)_1$
	$k_{thnf} = \frac{k_1 + 2k_{thnf} - 2\phi_1(k_{thnf} - k_1)}{k_1 + 2k_{thnf} + \phi_1(k_{thnf} - k_1)} \times k_{thnf}$ where
Thermal conductivity	$k_{thnf} = \frac{k_2 + 2k_{thnf} - 2\phi_2(k_{thnf} - k_2)}{k_2 + 2k_{thnf} + \phi_2(k_{thnf} - k_2)} \times k_{thnf}$ and $k_{thnf} = \frac{k_3 + 2k_f - 2\phi_3(k_f - k_3)}{k_3 + 2k_f + \phi_3(k_f - k_3)} \times k_f$

Table 2

Physical and thermal characteristics of the base fluid and nanoparticles [48,49].

Properties	Water	Alumina	Copper	Titanium dioxide
ρ (kg/m ³)	997.1	3970	8933	4250
C_p (J/kgK)	4179	765	385	686.2
k (W/mK)	0.613	40	400	8.9538
Pr	6.2	NA	NA	NA
ϕ	NA	1%	1%	1%

$$\frac{1}{Pr} \frac{1}{(\rho C_p)_{thnf} / (\rho C_p)_f} \left(\frac{k_{thnf}}{k_f} + \frac{4}{3} Rd \right) \theta' + (f + g)\theta' - \frac{1}{2} \beta \eta \theta' = 0, \quad (12)$$

subject to the boundary conditions

$$\left. \begin{aligned} f(0) = S, f'(0) = \lambda, g(0) = 0, g'(0) = \lambda, h(0) = 0, \theta(0) = 1, \\ f'(\eta) \rightarrow 0, g'(\eta) \rightarrow 0, h(\eta) \rightarrow 1, \theta(\eta) \rightarrow 0 \text{ as } \eta \rightarrow \infty, \end{aligned} \right\} \quad (13)$$

where, β is the unsteadiness parameter, Pr is the Prandtl number, and Rd is the radiation parameter, which is defined as [42,47]:

$$\beta = \frac{c}{a}, Rd = \frac{4\sigma^* T_{\infty}^3}{k_f k^*}, Pr = \frac{(\mu C_p)_f}{k_f}. \quad (14)$$

The physical quantities of practical interest are the skin friction coefficients C_{fx} (along x -axis), C_{fy} (along y -axis), and the local Nusselt number Nu_x [42]:

$$\left. \begin{aligned} C_{fx} = \frac{\mu_{thnf}}{\rho_f u_w^2(x)} \left(\frac{\partial u}{\partial z} \right)_{z=0}, C_{fy} = \frac{\mu_{thnf}}{\rho_f v_w^2(x)} \left(\frac{\partial v}{\partial z} \right)_{z=0}, \\ Nu_x = -\frac{x}{k_f(T_w - T_{\infty})} \left(k_{thnf} + \frac{16\sigma^* T_{\infty}^3}{3k^*} \right) \left(\frac{\partial T}{\partial z} \right)_{z=0}. \end{aligned} \right\} \quad (15)$$

By utilizing Eqs. (7) and (15), we derive the following:

$$\left. \begin{aligned} Re_x^{1/2} C_{fx} = \frac{\mu_{thnf}}{\mu_f} \left[f''(0) + \frac{U}{ax} h'(0) \right], Re_y^{1/2} C_{fy} = \frac{\mu_{thnf}}{\mu_f} g''(0), \\ Re_x^{-1/2} Nu_x = -\left(\frac{k_{thnf}}{k_f} + \frac{4}{3} Rd \right) \theta'(0), \end{aligned} \right\} \quad (16)$$

where $Re_x = u_w(x)x/v_f$ and $Re_y = v_w(y)y/v_f$ are the local Reynolds numbers.

3. Analytical solution for two-dimensional case

For the two-dimensional case, $g(\eta) = 0$, with $\phi_1 = \phi_2 = \phi_3 = 0$ (classical viscous fluid) and $\beta = 0$ (steady flow), Eq. (9) along with the boundary conditions (13) for $f(\eta)$ reduce to the following boundary value problem:

$$\left. \begin{aligned} f''' + ff'' - f'^2 = 0, \\ f(0) = S, f'(0) = \lambda, f'(\eta) \rightarrow 0 \text{ as } \eta \rightarrow \infty, \end{aligned} \right\} \quad (17)$$

and has the following exact analytical solution (see Roşca and Pop [50] and Wahid et al. [51])

$$f(\eta) = S + \frac{\lambda}{\alpha} (1 - e^{-\alpha \eta}) \text{ such that}$$

$$\left(S + \frac{\lambda}{\alpha} \right) > 0. \quad (18)$$

Hence, by substitution to boundary value problem (17), it gives

$$\alpha^2 - S\alpha - \lambda = 0, \quad (19)$$

and then

$$\alpha = \frac{1}{2} \left(S + \sqrt{S^2 + 4\lambda} \right), \quad (20)$$

so that

$$f''(0) = -\alpha\lambda. \quad (21)$$

Thus, we obtain from Eq. (20), as anticipated, $\lambda_c < -S^2/4$, where $\lambda_c < 0$ is the critical value of $\lambda < 0$, for which the boundary value problem (17) has physically realizable solutions in practice. We observe that when $\lambda = 1$ (stretching sheet), $\alpha = 1$ and $S = 0$, it results in from Eq. (21) that $f'(0) = -1$, which agrees with the solution obtained by Crane [52] for the first time.

4. Flow stability

The numerical solution for ODEs in Eqs. (9)–(13) in MATLAB utilizing the bvp4c solver involves providing an initial guess, which may result in different solutions for the same problem. This occurrence, known as the existence of multiple solutions, is common in flow problems involving shrinkable surfaces and has been observed in previous studies [37,39,42], particularly in flow over biaxial or bidirectional stretch/shrink surfaces. In pursuit of a comparable stability analysis, we embrace the subsequent similarity variables [42,47]:

$$\left. \begin{aligned} u &= \frac{1}{1-ct} \left[ax \frac{\partial f}{\partial \eta}(\eta, \tau) + Uh(\eta, \tau) \right], v = \frac{ay}{1-ct} \frac{\partial g}{\partial \eta}(\eta, \tau), \\ w &= -\sqrt{\frac{av_f}{1-ct}} [f(\eta, \tau) + g(\eta, \tau)], \\ \theta(\eta, \tau) &= \frac{T - T_\infty}{T_w - T_\infty}, \eta = z \sqrt{\frac{a}{v_f(1-ct)}}, \tau = \frac{at}{1-ct}, \end{aligned} \right\} \quad (22)$$

with τ as dimensionless time variable.

Substituting Eq. (22) into Eqs. (2)–(5), one should get

$$\left(\frac{\mu_{thnf}/\mu_f}{\rho_{thnf}/\rho_f} \right) \frac{\partial^3 f}{\partial \eta^3} + (f+g) \frac{\partial^2 f}{\partial \eta^2} - \left(\frac{\partial f}{\partial \eta} \right)^2 - \beta \left(\frac{\partial f}{\partial \eta} + \frac{1}{2} \eta \frac{\partial^2 f}{\partial \eta^2} \right) - (1+\beta\tau) \frac{\partial^2 f}{\partial \eta \partial \tau} = 0, \quad (23)$$

$$\left(\frac{\mu_{thnf}/\mu_f}{\rho_{thnf}/\rho_f} \right) H'' + h_0'(F_0 + G_0) + H_0'(f_0 + g_0) - (F_0'h_0 + f_0'H_0) - \beta \left(H_0' + \frac{1}{2} \eta H_0'' \right) + \gamma H_0' = 0, \quad (31)$$

$$\frac{1}{Pr} \frac{1}{(\rho C_p)_{thnf}/(\rho C_p)_f} \left(\frac{k_{thnf}}{k_f} + \frac{4}{3} Rd \right) Q_0'' + \theta_0'(F_0 + G_0) + Q_0'(f_0 + g_0) - \frac{1}{2} \beta \eta Q_0' + \gamma Q_0' = 0, \quad (32)$$

$$\left(\frac{\mu_{thnf}/\mu_f}{\rho_{thnf}/\rho_f} \right) \frac{\partial^3 g}{\partial \eta^3} + (f+g) \frac{\partial^2 g}{\partial \eta^2} - \left(\frac{\partial g}{\partial \eta} \right)^2 - \beta \left(\frac{\partial g}{\partial \eta} + \frac{1}{2} \eta \frac{\partial^2 g}{\partial \eta^2} \right) - (1+\beta\tau) \frac{\partial^2 g}{\partial \eta \partial \tau} = 0, \quad (24)$$

$$\left(\frac{\mu_{thnf}/\mu_f}{\rho_{thnf}/\rho_f} \right) \frac{\partial^2 h}{\partial \eta^2} + (f+g) \frac{\partial h}{\partial \eta} - h \frac{\partial f}{\partial \eta} - \beta \left(h + \frac{1}{2} \eta \frac{\partial h}{\partial \eta} \right) - (1+\beta\tau) \frac{\partial h}{\partial \tau} = 0, \quad (25)$$

$$\frac{1}{Pr} \frac{1}{(\rho C_p)_{thnf}/(\rho C_p)_f} \left(\frac{k_{thnf}}{k_f} + \frac{4}{3} Rd \right) \frac{\partial^2 \theta}{\partial \eta^2} + (f+g) \frac{\partial \theta}{\partial \eta} - \frac{1}{2} \beta \eta \frac{\partial \theta}{\partial \eta} - (1+\beta\tau) \frac{\partial \theta}{\partial \tau} = 0, \quad (26)$$

subject to the boundary conditions

$$\left. \begin{aligned} f(0, \tau) &= S, f'(0, \tau) = g'(0, \tau) = \lambda, g(0, \tau) = h(0, \tau) = 0, \theta(0, \tau) = 1, \\ f'(\eta, \tau) &= g'(\eta, \tau) = \theta(\eta, \tau) \rightarrow 0, h(\eta, \tau) \rightarrow 1 \text{ as } \eta \rightarrow \infty. \end{aligned} \right\} \quad (27)$$

Following this, we introduce the subsequent exponential perturbation functions (Weidman et al. [53]; Grosan and Pop [37]; Wahid et al. [47]):

$$\left. \begin{aligned} f(\eta, \tau) &= f_0(\eta) + e^{-\gamma\tau} F(\eta, \tau), \\ g(\eta, \tau) &= g_0(\eta) + e^{-\gamma\tau} G(\eta, \tau), \\ h(\eta, \tau) &= h_0(\eta) + e^{-\gamma\tau} H(\eta, \tau), \\ \theta(\eta, \tau) &= \theta_0(\eta) + e^{-\gamma\tau} Q(\eta, \tau), \end{aligned} \right\} \quad (28)$$

with f_0, g_0, h_0 and θ_0 as the steady flow solution that are relatively large compared to $F(\eta, \tau), G(\eta, \tau), H(\eta, \tau)$ and $Q(\eta, \tau)$, and γ is the eigenvalue that need to be solved. Applying Eq. (28) to Eqs. (23)–(27), and letting $\tau = 0$ so that $F(\eta, \tau) = F_0(\eta), G(\eta, \tau) = G_0(\eta), H(\eta, \tau) = H_0(\eta)$ and $Q(\eta, \tau) = Q_0(\eta)$, produces:

$$\left(\frac{\mu_{thnf}/\mu_f}{\rho_{thnf}/\rho_f} \right) F_0''' + f_0''(F_0 + G_0) + F_0''(f_0 + g_0) - 2F_0'f_0' - \beta \left(F_0' + \frac{1}{2} \eta F_0'' \right) + \gamma F_0' = 0, \quad (29)$$

$$\left(\frac{\mu_{thnf}/\mu_f}{\rho_{thnf}/\rho_f} \right) G_0''' + g_0''(F_0 + G_0) + G_0''(f_0 + g_0) - 2G_0'g_0' - \beta \left(G_0' + \frac{1}{2} \eta G_0'' \right) + \gamma G_0' = 0, \quad (30)$$

subject to the boundary conditions

$$\left. \begin{aligned} F_0(0) &= G_0(0) = F_0'(0) = G_0'(0) = H_0(0) = Q_0(0) = 0, \\ F_0'(\eta) &= G_0'(\eta) = H_0(\eta) = Q_0(\eta) = 0 \text{ as } \eta \rightarrow \infty. \end{aligned} \right\} \quad (33)$$

To solve this eigenvalue problem, a modification in the boundary conditions (33) is needed as suggested by Harris et al. [54], such that we alter $F_0'(\infty) \rightarrow 0$ to become $F_0''(0) = 1$. This alteration facilitates the numerical computation of γ when employing the bvp4c solver in MATLAB. To ascertain the stability of the solution, we examine the positivity or negativity of the generated smallest eigenvalues ($\gamma_1 < \gamma_2 < \gamma_3 \dots$). A positive smallest eigenvalue indicates solution stability, whereas a negative value denotes instability.

5. Numerical procedure (bvp4c)

The well-established MATLAB boundary value problem solver called bvp4c, with a 10^{-10} tolerance error is employed to attain a numerical solution for the systems of nonlinear ordinary differential equations (ODEs) presented in Eqs. (9)–(12), considering the specified boundary conditions (13). However, a prerequisite for this process involved reducing the system of ODEs, along with the boundary conditions, into a set of first-order ordinary differential equations through the introduction of new variables such that

$$\left. \begin{aligned} f &= y(1), f' = y(2), f'' = y(3), \\ g &= y(4), g' = y(5), g'' = y(6), \\ h &= y(7), h' = y(8), \\ \theta &= y(9), \theta' = y(10), \end{aligned} \right\} \quad (34)$$

so that Eqs. (9)–(13) transformed to

$$\left. \begin{aligned} f''' &= \frac{1}{\left(\frac{\mu_{thnf}}{\rho_{thnf}} / \frac{\mu_f}{\rho_f}\right)} \left[-(y(1)+y(4))y(3) + y(2)y(2) + \beta \left(y(2) + \frac{1}{2}\eta y(3) \right) \right], \\ g''' &= \frac{1}{\left(\frac{\mu_{thnf}}{\rho_{thnf}} / \frac{\mu_f}{\rho_f}\right)} \left[-(y(1)+y(4))y(6) + y(5)y(5) + \beta \left(y(5) + \frac{1}{2}\eta y(6) \right) \right], \\ h''' &= \frac{1}{\left(\frac{\mu_{thnf}}{\rho_{thnf}} / \frac{\mu_f}{\rho_f}\right)} \left[-(y(1)+y(4))y(8) + y(7)y(2) + \beta \left(y(7) + \frac{1}{2}\eta y(8) \right) \right], \\ \theta'' &= \frac{1}{\frac{1}{Pr} \frac{1}{(\rho C_p)_{thnf}} / (\rho C_p)_f \left(\frac{k_{thnf}}{k_f} + \frac{4}{3}Rd \right)} \left[-(y(1)+y(4))y(10) + \frac{1}{2}\beta \eta y(10) \right]. \end{aligned} \right\} \quad (35)$$

And, the boundary conditions from Eq. (13) become

$$\left. \begin{aligned} ya(1) - S, ya(2) - \lambda, ya(4), ya(5) - \lambda, ya(7), ya(9) - 1, \\ yb(2), yb(5), yb(7) - 1, yb(9), \end{aligned} \right\} \quad (36)$$

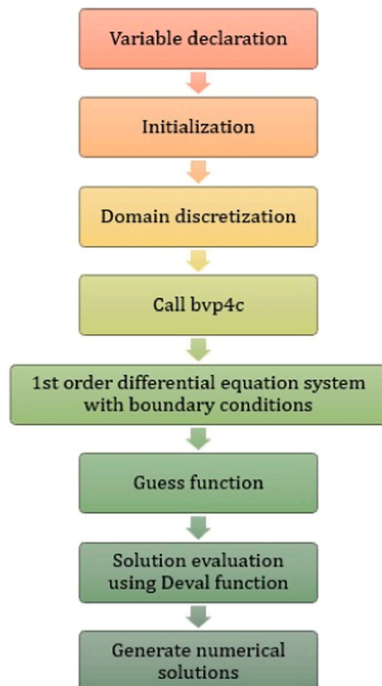


Fig. 2. Bvp4c procedure flowchart.

where a and b refers to the condition when $\eta = 0$ and $\eta \rightarrow \infty$ ($\eta_\infty = 15$). Following this transformation, the next step involved providing initial guesses for these new variables to facilitate the numerical solution process. The suitable initial guesses are important to generate the possible numerical solutions that asymptotically converge and satisfy the boundary condition. In this case, since we are interested in seeing whether the system can generate more than one solution, therefore, we provide two initial guesses to generate two non-unique numerical solutions. The flow chart of the general procedure in bvp4c is displayed in Fig. 2.

6. Results and discussion

The numerical investigation of the ODEs stated in Eqs. (9)–(12) subject to Eq. (13) stands as a pivotal aspect of this study. Employing a finite difference scheme within bvp4c solver (MATLAB), we elucidated the dynamics of the ternary hybrid nanofluid system by scrutinizing various physical quantities. Specifically, our focus delved into pivotal parameters, notably suction, thermal radiation, and the shrinking capacity, under a constant state of unsteadiness within a 1:1:1 vol fraction of alumina, copper, and titanium dioxide water-based ternary hybrid nanofluid composition. It is important to highlight that the chosen range of parameter values in this study is determined by their appropriateness for generating numerical solutions, and this selection is informed by references from existing studies.

The derived output from this numerical model was observed through key physical markers such as the local skin friction $f''(0)$, $h'(0)$, $g'(0)$, local Nusselt number $-\theta'(0)$, and the profiles of velocity $f(\eta)$, $h(\eta)$, $g(\eta)$ and temperature $\theta(\eta)$. Prior to the generation of these outputs, our model underwent a meticulous validation process. This validation comprised a thorough comparison between our numerical outputs and those derived from a comparable model. The corroborative results, outlined in Tables 3 and 4, clearly validate the correlation between our numerical solutions and the prior study. This validation process thus serves as a robust substantiation, firmly establishing the credibility and reliability of both our model and the employed numerical procedures.

The impact of several S on $f''(0)$, $g''(0)$, $h'(0)$ and $-\theta'(0)$ when $\lambda_c \leq \lambda \leq -0.3$, $\beta = -1$ and $Rd = 1$ is shown in Figs. 3–5, respectively. Two solutions emerge, denoted as the first solution and the second solution, both of which display opposite patterns of impact towards each other for the case of $f''(0)$, $g''(0)$, $h'(0)$, but not for $-\theta'(0)$. As the suction parameter S at the boundary shifts from 2.3 to 2.5, interesting patterns emerge in the distribution of $f''(0)$, $g''(0)$ for the first solution. Surprisingly, the second solution exhibits the reverse trend. Meanwhile, the distribution of $h'(0)$ in the first solution decreases as S increases, while the second solution mirrors the reverse pattern. Yet, the distribution of $-\theta'(0)$ shows a positive trend in both solutions as S increases within the ternary hybrid nanofluids system. Physically, the increment in suction could control the boundary layer by preventing thermal separation and reducing thermal resistance thus optimizing conditions for enhancing the heat transfer performance. Further, these findings also shed light on the control of boundary layer separation by manipulating S . Increasing S appears to delay the separation process, as depicted in the figures while decreasing S accelerates the separation. The application of these insights heavily depends on specific contexts. This is substantiated physically, as an escalation in the suction parameter indicates a greater extraction of fluid from the boundary layer. This mechanism adeptly regulates boundary layer thickness and alleviates adverse pressure gradients, thereby forestalling the initiation of turbulent flow and maintaining the laminar flow. Consideration of laminar flow conditions is crucial in heat exchangers, microchannel heat exchangers, fluidized bed heat transfer, and electronics cooling to ensure efficient and uniform heat transfer processes.

Fig. 6 displays the impact of several Rd on $-\theta'(0)$ when $\lambda_c \leq \lambda \leq -0.3$, $\beta = -1$ and $S = 2.5$. Two solutions derived from these findings

Table 3

Comparison of results when $f'(0) = 1$, and $S = \beta = \phi_{1,2,3} = 0$.

$g'(0) = \lambda$	Present			Wang [45]		
	$f'(0)$	$g'(0)$	$h'(0)$	$f'(0)$	$g'(0)$	$h'(0)$
0	-1.000000057	0.000000000	0.367882385	-1.0000	0.0000	0.3681
0.2	-1.039495196	-0.148736917	0.443395992	-1.0395	-0.1487	0.4435
0.4	-1.075788107	-0.349208657	0.507445110	-1.0758	-0.3492	0.5076
0.5	-1.093095018	-0.465204846	0.536714024	-1.0931	-0.4652	0.5368

Table 4

Comparison of results when $f'(0) = 1$, $Pr = Rd = 1$, $S = \beta = \phi_{1,2,3} = 0$.

$g'(0) = \lambda$	$\theta'(0)$	
	Present	Wang [45]
0.25	-0.665926193	-0.66593
0.5	-0.735332013	-0.73533
0.75	-0.796470695	-0.79647

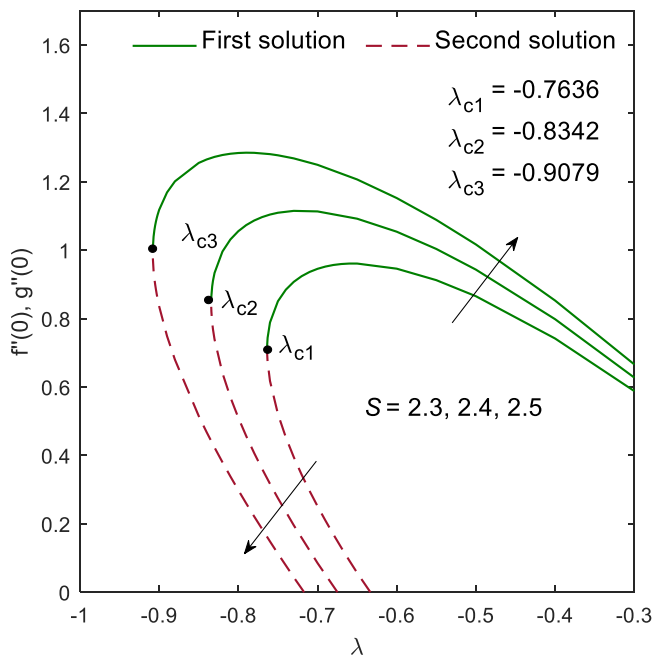


Fig. 3. Impact of suction on $f''(0), g''(0)$.

consistently exhibit a negative effect on $-\theta'(0)$ as Rd increases. Intriguingly, in the context of the fluid flow system, manipulating Rd fails to exert control over boundary layer separation, evidenced by the consistent critical point despite variations in Rd values. Generally, thermal radiation has minimal to no impact on the separation of the boundary layer process because it primarily affects the temperature profile rather than the velocity-driven dynamics leading to separation. Additionally, it is worth highlighting that Rd does not exert an influence on the skin friction as it lacks mathematical correlation with the momentum equations and might not be physically impacting the skin friction.

The impacts of S and Rd on the profiles of $f'(\eta), g'(\eta), h(\eta)$ and $\theta(\eta)$ are shown in Figs. 7–10, respectively. An increase in S leads to an augmented distribution profile of $f'(\eta), g'(\eta)$ concurrently reducing the momentum boundary layer thickness (first solution), while exhibiting an opposite trend for the second solution. Furthermore, in the context of $h(\eta)$, the first solution experiences a reduction as S increases, contrasting with the behavior observed in the second solution. Notably, both solutions demonstrate a negative impact on $\theta(\eta)$ as S increases, while the

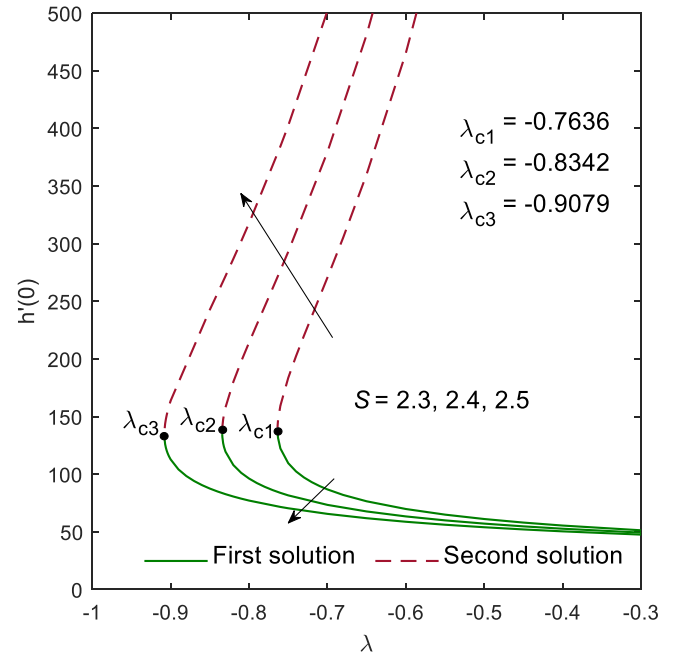


Fig. 4. Impact of suction on $h'(0)$.

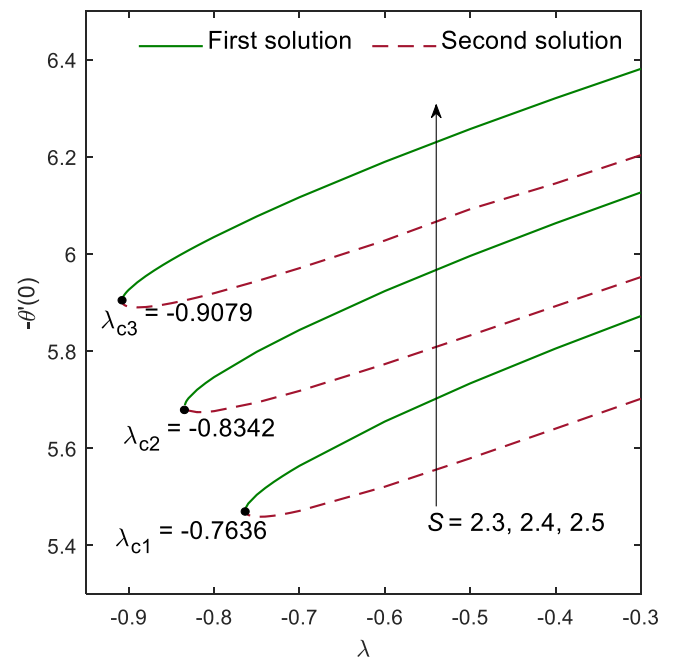
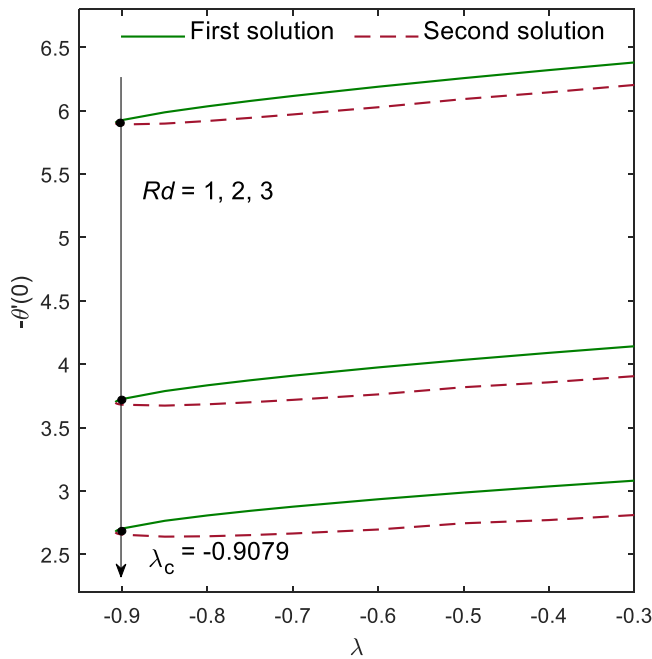
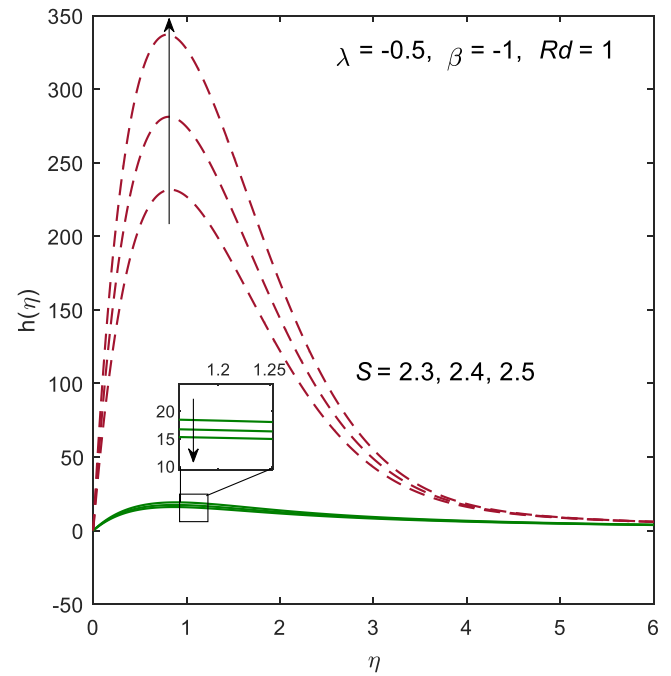
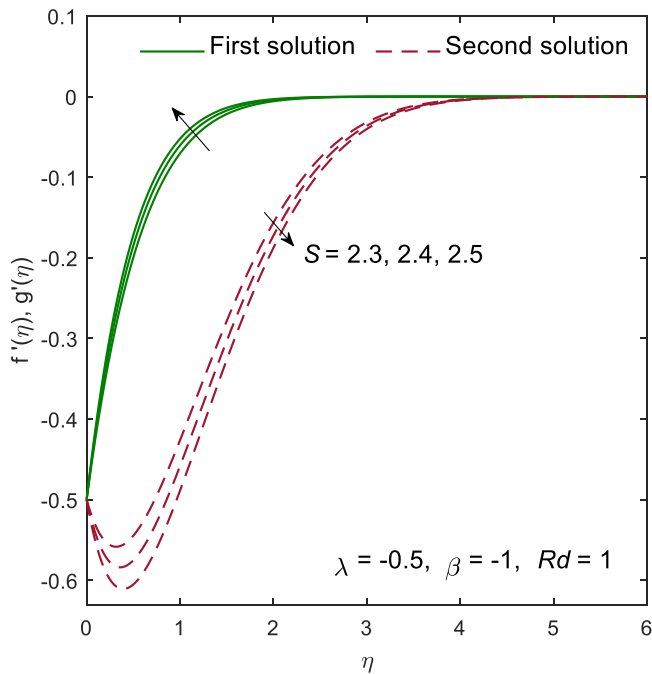
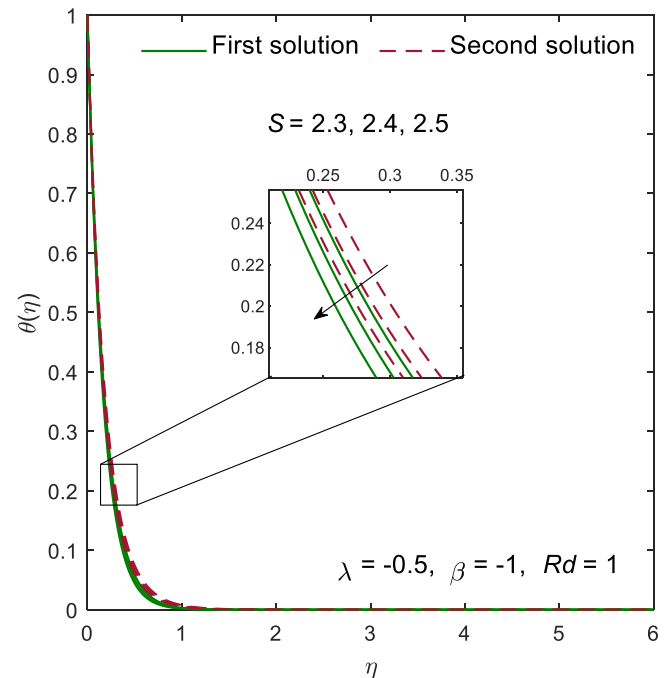


Fig. 5. Impact of suction on $-\theta'(0)$.

Fig. 6. Impact of thermal radiation on $-\theta'(0)$.Fig. 8. Impact of suction on $h(\eta)$.Fig. 7. Impact of suction on $f'(\eta), g'(\eta)$.Fig. 9. Impact of suction on $\theta(\eta)$.

thickness of the thermal boundary layer diminishes with S increments. For the impact of Rd , Fig. 10 illustrates that the increment in Rd amplifies $\theta(\eta)$ and correspondingly increases the thickness of the thermal boundary layer (for both solutions). However, the impact of Rd on $f'(\eta), g'(\eta), h(\eta)$ remains unavailable, primarily due to the mathematical and possibly physical insensitivity of Rd toward the velocity fluid flow system. It is vital to state that these observations regarding the impact of S and Rd on the profiles are presented under specific conditions where the shrinking parameter remains fixed at -0.5 , and the unsteadiness parameter maintains a deceleration constant of -1 .

Nevertheless, although our model generates two solutions, it is imperative to highlight that only the first solution is stable after we have

gone through the stability analysis. The findings in Table 5 corroborate this analysis: the first solution manifests positive γ_1 , affirming its stability. Conversely, the second solution exhibits the negative γ_1 , establishing its instability. It is also observable from Table 5 that $\gamma_1 \rightarrow 0$ as $\lambda \rightarrow \lambda_c$. In the first solution, $+\gamma_1 \rightarrow 0$ indicates decay in perturbations, signifying stability. Conversely, in the second solution, $-\gamma_1 \rightarrow 0$ indicates growth in perturbations, signifying instability. This stability finding also aligns with existing studies, as supported by [39,42]. However, though the second solution is not stable, we still report it for future reference.

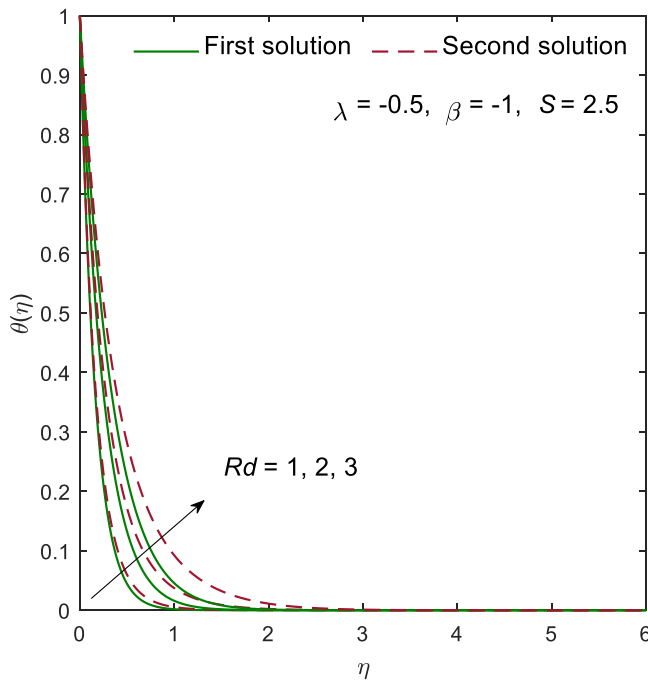


Fig. 10. Impact of thermal radiation on $\theta(\eta)$.

Table 5

Tabulation of smallest eigenvalues for several λ when $\beta = -1, Rd = 1, S = 2.5$.

λ	γ_1	
	First solution	Second solution
-0.9	0.2341	-0.2211
-0.907	0.0811	-0.0795
-0.9079	0.0246	-0.0244

7. Conclusion

The present numerical exploration investigating the intricate interplay of unsteady flow and heat transfer phenomena over a permeable biaxial shrinking sheet immersed in a ternary hybrid nanofluid, accounting for thermal radiation effects, has unraveled significant insights. The initial formulation of the model as PDEs, transformed adeptly into ODEs via established similarity transformations, enabled a comprehensive numerical analysis using the finite difference scheme facilitated by the bvp4c solver in MATLAB. A notable outcome of this analysis was the revelation of two potential solutions, of which only one exhibited physical stability. The key findings can be concluded as below:

- Augmenting the suction parameter enhances the local skin friction in both x and y directions.
- A remarkable 9% delay in the boundary layer separation of the ternary hybrid nanofluid is achieved by incrementing the suction parameter by 4%.
- Thermal radiation showed no significant impact on boundary layer separation.
- Increased suction correlates with higher velocities in both x and y directions, while extra suction reduces system temperature.
- Elevated thermal radiation notably raises the temperature within the ternary hybrid nanofluid system.
- Enlarging the boundary suction parameter and reducing thermal radiation show promise in augmenting heat transfer within specified conditions of ternary hybrid nanofluids.

Yet, it is crucial to note that the current findings might not

universally apply to all system configurations. Therefore, it is encouraged to further advance this work by exploring diverse geometries and parameter impositions, either through numerical investigations or experimental validations, for future research. Such efforts hold the promise of enriching our comprehension and refining the model, offering invaluable insights applicable to diverse practical scenarios in thermal management and engineering.

CRediT authorship contribution statement

Ioan Pop: Conceptualization, Writing – original draft. **Najiyah Safwa Khashi'ie:** Methodology, Software. **Rusya Iryanti Yahaya:** Writing – review & editing. **Norihan Md Arifin:** Funding acquisition, Supervision. **Nur Syahirah Wahid:** Formal analysis, Investigation, Methodology, Writing – review & editing.

Declaration of Competing Interest

None.

Acknowledgment

The authors acknowledge the support provided by Universiti Putra Malaysia [GP-GPB 9711400], Babeş-Bolyai University, and Universiti Teknikal Malaysia Melaka. The work by Ioan Pop has been supported by Grant PN-III-P4-PCE-2021-0993, UEFISCDI, Romania.

References

- [1] S. Bilal, I.A. Shah, M. Ramzan, K.S. Nisar, A. Elfakhany, E.M. Eed, H.A. S. Ghazwani, Significance of induced hybridized metallic and non-metallic nanoparticles in single-phase nano liquid flow between permeable disks by analyzing shape factor, *Sci. Rep.* 12 (2022) 3342, <https://doi.org/10.1038/s41598-022-07251-y>.
- [2] M. Jameel, Z. Shah, M. Rooman, M.H. Alshehri, N. Vranceanu, Entropy generation analysis on Darcy-Forchheimer Maxwell nanofluid flow past a porous stretching sheet with threshold Non-Fourier heat flux model and Joule heating, *Case Stud. Therm. Eng.* 52 (2023) 103738, <https://doi.org/10.1016/j.csite.2023.103738>.
- [3] H. Adun, D. Kavaz, M. Dagbasi, Review of ternary hybrid nanofluid: Synthesis, stability, thermophysical properties, heat transfer applications, and environmental effects, *J. Clean. Prod.* 328 (2021) 129525, <https://doi.org/10.1016/j.jclepro.2021.129525>.
- [4] T. Elnaqeeb, I.L. Animasaun, N.A. Shah, Ternary-hybrid nanofluids: significance of suction and dual-stretching on three-dimensional flow of water conveying nanoparticles with various shapes and densities, *Z. f. uR. Naturforsch. A* 76 (2021) 231–243, <https://doi.org/10.1515/zna-2020-0317>.
- [5] H. Adun, D. Kavaz, M. Dagbasi, H. Umar, I. Wole-Osho, An experimental investigation of thermal conductivity and dynamic viscosity of Al_2O_3 -ZnO-Fe $3O_4$ ternary hybrid nanofluid and development of machine learning model, *Powder Technol.* 394 (2021) 1121–1140, <https://doi.org/10.1016/j.powtec.2021.09.039>.
- [6] J. Mohammed Zayan, A.K. Rasheed, A. John, M. Khalid, A.F. Ismail, A. Aabid, M. Baig, Investigation on rheological properties of water-based novel ternary hybrid nanofluids using experimental and taguchi method, *Materials* 15 (2021) 28, <https://doi.org/10.3390/ma15010028>.
- [7] M. Sepehrnia, H. Maleki, M. Karimi, E. Nabati, Examining rheological behavior of CeO 2 -GO-SA/10W40 ternary hybrid nanofluid based on experiments and COMBI/ANN/RSM modeling, *Sci. Rep.* 12 (2022) 22054, <https://doi.org/10.1038/s41598-022-26253-4>.
- [8] M. Bilal, I. Ullah, M.M. Alam, W. Weera, A.M. Galal, Numerical simulations through PCM for the dynamics of thermal enhancement in ternary MHD hybrid nanofluid flow over plane sheet, cone, and wedge, *Symmetry* 14 (2022) 2419, <https://doi.org/10.3390/sym14112419>.
- [9] Z. Mahmood, Z. Iqbal, M.A. Alyami, B. Alqahtani, M.F. Yassen, U. Khan, Influence of suction and heat source on MHD stagnation point flow of ternary hybrid nanofluid over convectively heated stretching/shrinking cylinder, *168781322211262*, *Adv. Mech. Eng.* 14 (2022), <https://doi.org/10.1177/16878132221126278>.
- [10] S. Manjunatha, V. Puneeth, B.J. Gireesha, AliJ. Chamkha, Theoretical study of convective heat transfer in ternary nanofluid flowing past a stretching sheet, *J. Appl. Comput. Mech.* (2021), <https://doi.org/10.22055/jacm.2021.37698.3067>.
- [11] Z. Mahmood, N.A. Ahammad, S.E. Alhazmi, U. Khan, M.Z. Bani-Fwaz, Ternary hybrid nanofluid near a stretching/ shrinking sheet with heat generation/absorption and velocity slip on unsteady stagnation point flow, *Int. J. Mod. Phys. B* 36 (2022) 2250209, <https://doi.org/10.1142/S0217979222502095>.
- [12] S. Nandi, K. Vajravelu, Analysis of entropy generation in Carreau ternary hybrid nanofluid flow over a stretching sheet, *Numer. Heat. Transf. Part Appl.* (2023) 1–25, <https://doi.org/10.1080/10407782.2023.2233730>.

- [13] A. Zeeshan, M.I. Khan, R. Ellahi, M. Marin, Computational intelligence approach for optimising mhd casson ternary hybrid nanofluid over the shrinking sheet with the effects of radiation, *Appl. Sci.* 13 (2023) 9510, <https://doi.org/10.3390/app13179510>.
- [14] S. Riaz, M.F. Afzaal, Z. Wang, A. Jan, U. Farooq, Numerical heat transfer of non-similar ternary hybrid nanofluid flow over linearly stretching surface, *Numer. Heat. Transf. Part Appl.* (2023) 1–15, <https://doi.org/10.1080/10407782.2023.2251093>.
- [15] K.V. Nagaraja, U. Khan, J.K. Madhukesh, A.M. Hassan, B.C. Prasannakumara, N. Ben Kahla, S. Elattar, J. Singh Chohan, Heat and mass transfer analysis of assisting and opposing radiative flow conveying ternary hybrid nanofluid over an exponentially stretching surface, *Sci. Rep.* 13 (2023) 14795, <https://doi.org/10.1038/s41598-023-41916-6>.
- [16] M. Mumtaz, S. Islam, H. Ullah, Z. Shah, Chemically reactive MHD convective flow and heat transfer performance of ternary hybrid nanofluid past a curved stretching sheet, *J. Mol. Liq.* 390 (2023) 123179, <https://doi.org/10.1016/j.molliq.2023.123179>.
- [17] S.U. Jan, U. Khan, M.A. El-Rahman, S. Islam, A.M. Hassan, A. Ullah, Effect of variable thermal conductivity of ternary hybrid nanofluids over a stretching sheet with convective boundary conditions and magnetic field, *Results Eng.* 20 (2023) 101531, <https://doi.org/10.1016/j.rineng.2023.101531>.
- [18] L.L. Animasaun, N.A. Shah, A. Wakif, B. Mahanthesh, R. Sivaraj, O.K. Koriko, *Ratio of Momentum Diffusivity to Thermal Diffusivity: Introduction, Meta-analysis, and Scrutinization*, first ed., Chapman and Hall/CRC, Boca Raton, 2022, 10.1201/9781003217374.
- [19] J. Meseguer, I. Pérez-Grande, A. Sanz-Andrés, Thermal radiation heat transfer. in: *Spacecr. Therm. Control*, Elsevier, 2012, pp. 73–86, <https://doi.org/10.1533/9780857096081.73>.
- [20] S. Basu, Z.M. Zhang, C.J. Fu, Review of near-field thermal radiation and its application to energy conversion, *Int. J. Energy Res.* 33 (2009) 1203–1232, <https://doi.org/10.1002/er.1607>.
- [21] M. Sajid, T. Hayat, Influence of thermal radiation on the boundary layer flow due to an exponentially stretching sheet, *Int. Commun. Heat. Mass Transf.* 35 (2008) 347–356, <https://doi.org/10.1016/j.icheatmasstransfer.2007.08.006>.
- [22] S. Mishra, R. Dalai, K. Swain, Effects of copper and titania nanoparticles on MHD 3D rotational flow over an elongating sheet with convective thermal boundary condition, *Int. J. Ambient Energy* 44 (2023) 381–389, <https://doi.org/10.1080/01430750.2022.2127892>.
- [23] G. Mandal, D. Pal, Stability analysis of radiative-magnetic hybrid nanofluid slip flow due to an exponentially stretching/shrinking permeable sheet with heat generation, *Int. J. Ambient Energy* 44 (2023) 1349–1360, <https://doi.org/10.1080/01430750.2023.2173651>.
- [24] A.M. Alqahtani, M. Bilal, A. Ali, T.R. Alsenani, S.M. Eldin, Numerical solution of an electrically conducting spinning flow of hybrid nanofluid comprised of silver and gold nanoparticles across two parallel surfaces, *Sci. Rep.* 13 (2023) 7180, <https://doi.org/10.1038/s41598-023-33520-5>.
- [25] K. Swain, S.M. Ibrahim, G. Dharmiah, S. Noeiaghdam, Numerical study of nanoparticles aggregation on radiative 3D flow of maxwell fluid over a permeable stretching surface with thermal radiation and heat source/sink, *Results Eng.* 19 (2023) 101208, <https://doi.org/10.1016/j.rineng.2023.101208>.
- [26] K.A.M. Alharbi, M. Bilal, A. Ali, S.M. Eldin, A.F. Soliman, M.U. Rahman, Stagnation point flow of hybrid nanofluid flow passing over a rotating sphere subjected to thermophoretic diffusion and thermal radiation, *Sci. Rep.* 13 (2023) 19093, <https://doi.org/10.1038/s41598-023-46353-z>.
- [27] N.H. Hamad, M. Bilal, A. Ali, S.M. Eldin, M. Sharaf, M.U. Rahman, Energy transfer through third-grade fluid flow across an inclined stretching sheet subject to thermal radiation and Lorentz force, *Sci. Rep.* 13 (2023) 19643, <https://doi.org/10.1038/s41598-023-46428-x>.
- [28] C.Y. Wang, The three-dimensional flow due to a stretching flat surface, *Phys. Fluids* 27 (1984) 1915, <https://doi.org/10.1063/1.864868>.
- [29] B. Mahanthesh, B.J. Gireesha, R.S.R. Gorla, F.M. Abbasi, S.A. Shehzad, Numerical solutions for magnetohydrodynamic flow of nanofluid over a bidirectional non-linear stretching surface with prescribed surface heat flux boundary, *J. Magn. Mater.* 417 (2016) 189–196, <https://doi.org/10.1016/j.jmmm.2016.05.051>.
- [30] G.K. Ramesh, B.C. Prasannakumara, B.J. Gireesha, S.A. Shehzad, F.M. Abbasi, Three dimensional flow of Maxwell fluid with suspended nanoparticles past a bidirectional porous stretching surface with thermal radiation, *Therm. Sci. Eng. Prog.* 1 (2017) 6–14, <https://doi.org/10.1016/j.tsep.2017.02.006>.
- [31] I. Ahmad, M. Faisal, T. Javed, Magneto-nanofluid flow due to bidirectional stretching surface in a porous medium, *Spec. Top. Rev. Porous Media Int. J.* 10 (2019) 457–473, <https://doi.org/10.1615/SpecialTopicsRevPorousMedia.2019029445>.
- [32] I. Ahmad, I. Khurshid, M. Faisal, T. Javed, Z. Abbas, Mixed convective flow of an Oldroyd-B nanofluid impinging over an unsteady bidirectional stretching surface with the significances of double stratification and chemical reaction, *SN Appl. Sci.* 2 (2020) 1599, <https://doi.org/10.1007/s42452-020-03430-6>.
- [33] I. Ahmad, M. Faisal, T. Javed, Unsteady flow of walters-b magneto-nanofluid over a bidirectional stretching surface in a porous medium with heat generation, *Spec. Top. Rev. Porous Media Int. J.* 12 (2021) 49–70, <https://doi.org/10.1615/SpecialTopicsRevPorousMedia.2020034320>.
- [34] N. Joshi, H. Upreti, A.K. Pandey, M. Kumar, Heat and mass transfer assessment of magnetic hybrid nanofluid flow via bidirectional porous surface with volumetric heat generation, *Int. J. Appl. Comput. Math.* 7 (2021) 64, <https://doi.org/10.1007/s40819-021-00999-3>.
- [35] M. Ramzan, H. Gul, M.Y. Malik, H.A.S. Ghazwani, Entropy minimization analysis of a partially ionized casson nanofluid flow over a bidirectional stretching sheet with surface catalyzed reaction, *Arab. J. Sci. Eng.* 47 (2022) 15209–15221, <https://doi.org/10.1007/s13369-021-06492-9>.
- [36] B. Ishfaq, S. Nadeem, J. Alzabut, Effects of variable magnetic field and partial slips on the dynamics of Sutterby nanofluid due to biaxially exponential and nonlinear stretchable sheets, *Heliyon* 9 (2023) e17921, <https://doi.org/10.1016/j.heliyon.2023.e17921>.
- [37] T. Groşan, I. Pop, Flow and heat transfer over a permeable biaxial stretching/shrinking sheet in a nanofluid, *Neural Comput. Appl.* 32 (2020) 4575–4582, <https://doi.org/10.1007/s00521-018-3770-0>.
- [38] N. Khashi'ie, N.C. Roşca, A.V. Roşca, I. Pop, Dual solutions on MHD radiative three-dimensional bidirectional nanofluid flow over a non-linearly permeable shrinking sheet, *Alex. Eng. J.* 71 (2023) 401–411, <https://doi.org/10.1016/j.aej.2023.03.066>.
- [39] I. Waini, A. Ishak, I. Pop, Hybrid nanofluid flow and heat transfer over a permeable biaxial stretching/shrinking sheet, *Int. J. Numer. Methods Heat. Fluid Flow.* 30 (2019) 3497–3513, <https://doi.org/10.1108/HFF-07-2019-0557>.
- [40] N.A. Zainal, R. Nazar, K. Naganthran, I. Pop, Heat generation/absorption effect on MHD flow of hybrid nanofluid over bidirectional exponential stretching/shrinking sheet, *Chin. J. Phys.* 69 (2021) 118–133, <https://doi.org/10.1016/j.cjph.2020.12.002>.
- [41] M. Yasir, M. Sarfraz, M. Khan, A.K. Alzahrani, M.Z. Ullah, Estimation of dual branch solutions for Homann flow of hybrid nanofluid towards biaxial shrinking surface, *J. Pet. Sci. Eng.* 218 (2022) 110990, <https://doi.org/10.1016/j.petrol.2022.110990>.
- [42] R.I. Yahaya, M.S. Mustafa, N. Md Arifin, I. Pop, F. Md Ali, S.S.P. Mohamed Isa, Hybrid nanofluid flow past a biaxial stretching/shrinking permeable surface with radiation effect: stability analysis and heat transfer optimization, *Chin. J. Phys.* 85 (2023) 402–420, <https://doi.org/10.1016/j.cjph.2023.06.003>.
- [43] S. Manjunatha, V. Puneeth, A.K. Baby, C.S. Vishalakshi, Examination of thermal and velocity slip effects on the flow of blood suspended with aluminum alloys over a bi-directional stretching sheet: the ternary nanofluid model, *Waves Random Complex Media* (2022) 1–18, <https://doi.org/10.1080/17455030.2022.2056260>.
- [44] S. Choudhary, R. Mehta, N. Alessa, S. Jangid, M. Venkateswar Reddy, Thermal analysis on kerosene oil-based two groups of ternary hybrid nanoparticles (CNT-Gr-Fe3O4 and MgO-Cu-Au) mix flow over a bidirectional stretching sheet: a comparative approach, *J. Eng.* 2023 (2023) 1–20, <https://doi.org/10.1155/2023/8828300>.
- [45] C.Y. Wang, Uniform flow over a bi-axial stretching surface, *J. Fluids Eng.* 137 (2015) 045502, <https://doi.org/10.1115/1.4029447>.
- [46] S.S.U. Devi, S.P.A. Devi, Numerical investigation of three-dimensional hybrid Cu-Al₂O₃/water nanofluid flow over a stretching sheet with effecting Lorentz force subject to Newtonian heating, *Can. J. Phys.* 94 (2016) 490–496, <https://doi.org/10.1139/cjp-2015-0799>.
- [47] N.S. Wahid, N.M. Arifin, N.S. Khashi'ie, I. Pop, Three-dimensional unsteady radiative hybrid nanofluid flow through a porous space over a permeable shrinking surface, *Chin. J. Phys.* 85 (2023) 196–211, <https://doi.org/10.1016/j.cjph.2023.07.016>.
- [48] H.F. Oztop, E. Abu-Nada, Numerical study of natural convection in partially heated rectangular enclosures filled with nanofluids, *Int. J. Heat. Fluid Flow.* 29 (2008) 1326–1336, <https://doi.org/10.1016/j.jheatfluidflow.2008.04.009>.
- [49] N.S. Khashi'ie, N.M. Arifin, N.S. Wahid, I. Pop, Insight into unsteady separated stagnation point flow of hybrid nanofluids subjected to an electro-magnetohydrodynamics riga plate, *Magnetochemistry* 9 (2023) 46, <https://doi.org/10.3390/magnetochemistry9020046>.
- [50] N.C. Roşca, I. Pop, Unsteady boundary layer flow over a permeable curved stretching/shrinking surface, *Eur. J. Mech. - B Fluids* 51 (2015) 61–67, <https://doi.org/10.1016/j.euromechflu.2015.01.001>.
- [51] N.S. Wahid, N.M. Arifin, N.S. Khashi'ie, I. Pop, Mixed convection MHD hybrid nanofluid over a shrinking permeable inclined plate with thermal radiation effect, *Alex. Eng. J.* 66 (2023) 769–783, <https://doi.org/10.1016/j.aej.2022.10.075>.
- [52] L.J. Crane, Flow past a stretching plate, *Z. F. üR. Angew. Math. Phys. ZAMP* 21 (1970) 645–647, <https://doi.org/10.1007/BF01587695>.
- [53] P.D. Weidman, D.G. Kubitschek, A.M.J. Davis, The effect of transpiration on self-similar boundary layer flow over moving surfaces, *Int. J. Eng. Sci.* 44 (2006) 730–737, <https://doi.org/10.1016/j.jengsci.2006.04.005>.
- [54] S.D. Harris, D.B. Ingham, I. Pop, Mixed convection boundary-layer flow near the stagnation point on a vertical surface in a porous medium: brinkman model with slip, *Transp. Porous Media* 77 (2009) 267–285, <https://doi.org/10.1007/s11242-008-9309-6>.